Atmospheric Environment 226 (2020) 117404

Contents lists available at ScienceDirect

Atmospheric Environment

journal homepage: http://www.elsevier.com/locate/atmosenv

Formation of atmospheric molecular clusters of methanesulfonic acid–Diethylamine complex and its atmospheric significance

Cai-Xin Xu [a], Shuai Jiang [a,*], Yi-Rong Liu [a], Ya-Juan Feng [a], Zi-Hang Wang [a], Teng Huang [b], Yu Zhao [a], Jie Li [a], Wei Huang [a,b,c,**]

[a] School of Information Science and Technology, University of Science and Technology of China, Hefei, Anhui, 230026, China
[b] Laboratory of Atmospheric Physico-Chemistry, Anhui Institute of Optics & Fine Mechanics, Chinese Academy of Sciences, Hefei, Anhui, 230031, China
[c] Center for Excellent in Urban Atmospheric Environment, Institute of Urban Environment, Chinese Academy of Sciences, Xiamen, Fujian, 361021, China

HIGHLIGHTS

- A possible role in new particle formation in the marine atmosphere.
- MSA-DEA clusters with a similar number of acids and amines are more stable.
- Proton transfer enhances the stability of MSA–DEA clusters.
- MSA is more strongly bound in MSA-DEA clusters than DEA.

ARTICLE INFO

Keywords:
New particle formation
Diethylamine
Kinetic analysis
Proton transfer
Nucleation capability

ABSTRACT

Field observations in a marine atmospheric environment imply the occurrence of significant concentrations of dimethylamine (DMA) and diethylamine (DEA) as well as methanesulfonic acid (MSA) in particulate formation. Among these particulates, studies on the interaction of MSA with DMA are well known; however, fundamental studies relating to the environmental impact of DEA on aerosol formation and its nucleation ability relative to the known ones are lacking. In this research, quantum chemical calculations and cluster kinetic modeling were used to analyze the aerosol formation potential of the reaction of DEA with MSA. Structural and thermodynamic evidence demonstrate a strong clustering stability in the processes of new particle formation (NPF). Driven by proton transfer, the clusters exhibit a low free-energy barrier distributed along the diagonal. The results of cluster kinetic analysis indicate that the aerosol formation potential of the MSA-DEA system at the parts per trillion (ppt) level is inferior to that of sulfuric acid (SA)–DMA, and slightly superior to that of SA–methylamine (MA) but far superior to that of MSA–DMA, implying a relatively strong nucleation capability for MSA-DEA system. This result implies that the MSA-DEA system plays a potentially significant role in NPF in the marine environment.

1. Introduction

Marine aerosols are one of the most important natural aerosol systems in the world (Hinds, 2012; Fitzgerald, 1991), and play an important role in biogeochemical cycles (Paytan et al., 2009), the Earth's radiation and ecosystems (Palve et al., 2018), and global and regional air quality (Muñiz-Unamunzaga et al., 2018). New particle formation (NPF) is an essential process in aerosol formation and makes a significant contribution to atmospheric cloud condensation nuclei (CCN) (Kulmala, 2003; Charlson et al., 2001). A typical NPF event consists of two different phases (Wang et al., 2010; Temelso et al., 2012; Zhang et al., 2011; Zhang, 2010): (1) the formation of the critical nucleus, and (2) the growth of critical nucleus to a detectable size (2–3 nm). Many studies have been performed on the initial nucleation mechanism, however, understanding of the source of nucleation and the growth process at a molecular level remains incomplete (Kirkby et al., 2016; Yu et al., 2012; Tröstl et al., 2016; Kulmala et al., 2012; Liu et al., 2017, 2018a; van Pinxteren et al., 2019).

Diethylamine (DEA) is known to be closely linked to ocean biota emissions (Sorooshian et al., 2009). and is widely distributed in the

* Corresponding author.
** Corresponding author. School of Information Science and Technology, University of Science and Technology of China, Hefei, Anhui, 230026, China.
E-mail addresses: shuaijiang@ustc.edu.cn (S. Jiang), huangwei6@ustc.edu.cn (W. Huang).

https://doi.org/10.1016/j.atmosenv.2020.117404
Received 17 October 2019; Received in revised form 6 March 2020; Accepted 9 March 2020
Available online 12 March 2020

marine environment (Sorooshian et al., 2009; Müller et al., 2009; Facchini et al., 2008; Rinaldi et al., 2010). A study by Sorooshian et al. (2009) showed that enhanced chloroplast A levels and wind speeds were consistent with higher particulate concentrations of DEA and methanesulfonic acid (MSA). The relationship between chloroplast A and the average CCN concentration demonstrated that marine biological activity resulted in more numerous cloud drops. Owing to a significantly higher concentration of DEA measured during a period of high marine biological activity, this compound is considered as an important product of marine biological activity, and its role and involvement in NPF in the atmosphere warrant investigation. Other studies highlighting the links between DEA, marine biota, and aerosols have been reported (Müller et al., 2009; Rinaldi et al., 2010); hence, it is important to pursue research on NPF containing DEA.

Previous studies have demonstrated that sulfuric acid (SA) is an important component of atmospheric aerosols (Zhang, 2010; Zheng et al., 2010; Sipilä et al., 2010; Berndt et al., 2005; Yao et al., 2018). The binary nucleation of SA and water (W) was once considered to be the main source of NPF in the atmosphere (Young et al., 2008; Brus et al., 2010; Kürten et al., 2015). However, binary homogeneous nucleation of SA and water is not an adequate interpretation of the actual atmospheric nucleation process, and other substances have been proposed as being involved in nucleation processes (Aalto et al., 2001; Almeida et al., 2013). Organic compounds are also an important source of atmospheric aerosol formation (Zhang et al., 2004). Studies on organic compounds including amines (Kurtén et al., 2008; Kupiainen et al., 2012; Loukonen et al., 2010; Nadykto et al., 2011, 2014, 2015; Elm et al., 2016; Henschel et al., 2014), organic acids (Zhang et al., 2004; Elm et al., 2017), and amino acids (Elm et al., 2013; Wang et al., 2016), are well known, and early modeling studies have shown that amines and SA can form stable clusters (Kurtén et al., 2008; Loukonen et al., 2010).

Apart from SA, the oxidation of organosulfur compounds (OSCs) produces another major nucleating precursor, MSA, and, given the environmental regulatory restrictions on SO_2 emissions, the contribution of MSA to NPF will become more significant, especially for the marine environment (Perraud et al., 2015). The production of MSA is related to various processes including biological processes, biomass burning, and the oxidation of organosulfur compounds in industrial and agricultural activities (Bates et al., 1992; VanderGheynst et al., 1998; Rosenfeld et al., 2001; Meinardi et al., 2003). Gas phase MSA has been measured in the atmosphere at a concentration of 10^5–10^7 cm^{-3}, which is about 10–100% of that of SA (Eisele and Tanner, 1993; Berresheim et al., 2002). Previous studies have shown that MSA is an important precursor that contributes to both NPF and particle growth in the atmosphere (Sorooshian et al., 2009; Facchini et al., 2008; Dawson et al., 2012; Ezell et al., 2014; Chen et al., 2015a; Zorn et al., 2008; Gaston et al., 2010; Hopkins et al., 2008; Kreidenweis and Seinfeld, 1967). Research on MSA to promote NPF is quite widespread and includes binary nucleation systems of MSA with amines or ammonia (Dawson et al., 2012; Chen et al., 2015a, 2015b), and ternary nucleation systems such as MSA–SA–DMA (Bork et al., 2014), MSA–NH_3/amines–W (Dawson et al., 2012; Chen et al., 2015a; Chen and Finlayson-Pitts, 2016; Li et al., 2007) and MSA–SA–W, (Hanson, 2005; Napari et al., 2002). Experimental and theoretical studies by the Finlayson-Pitts group have shown that MSA can form particles with amines (Dawson et al., 2012). Therefore, given the potential of MSA to form clusters with amines and considering the relationship between DEA and aerosols in the atmosphere, it is clearly essential to study the process of NPF of MSA and DEA.

2. Methods

The initial geometries of the $(MSA)_m(DEA)_n$ ($m = 0-3$ and $n = 0-3$) clusters were obtained by using the Basin-Hopping (BH) algorithm (Huang et al., 2010; Wales and Doye, 1997; Yoon et al., 2007) combined with the semi empirical PM7 (Hostaš et al., 2013) implemented in MOPAC 2016 (Maia et al., 2012). Previous work in our group used this method to calculate the infrared spectra and vertical detachment energy of atmospheric related clusters, which were compared with experimental values, and the stability of the computational method was verified (Jiang et al., 2014; Liu et al., 2014). Also, we performed multiple Basin-Hopping searches by changing different parameters mainly including the temperature for funnel sampling and bond change for structure change extent, and when the last three searches provided the same global minimum, we believed that the potential global minimum was characterized and the search processes should be stopped. At last, all searched structures were further verified by our chemical intuition considering the coordination number as well as binding sites. The larger the cluster the more the BH searches, and the more isomers per search. The search was stopped when multiple search results appear to contain the same 30 lowest energy structures. Excessive number of structures result in duplicates of the optimized isomers, but deficient number of structures cause some important isomers to be omitted. In light of previous experience, we selected 30 conformers here. Therefore, the initial 30 lowest-energy geometries for all structures from BH search were selected for optimization (Wen et al., 2018). All the selected results were optimized at the M06–2X/6–31++G(d,p) level of theory (Bork et al., 2014; Walker et al., 2013). The M06–2X method has been verified to give a good performance for a large number of atmospheric cluster containing common organic acids (Bork et al., 2014; Zhao and Truhlar, 2008), especially for the similar results with experimental results (Elm et al., 2012) and theoretical level of DLPNO–CCSD(T)/aug–cc–pVTZ (Elm and Kristensen, 2017). According to the study of Bork et al. (2014), for the $(MSA)_2$ complex, M06-2X overestimates the Gibbs free energies by 1.54 kcal/mol; for MSA-DMA cluster, a slight underestimation of 0.77 kcal/mol is observed, and errors in binding energies of molecular clusters with both acid–acid and acid–base bonds have tendencies to cancel out rather than accumulate. Therefore, it is reasonable to believe that the apparent over-binding of the M06-2X functional is severely less than 1.54 kcal/mol These all indicate reliable results in the MSA–-amine clusters using the M06–2X functional. Elm et al. (Elm and Mikkelsen, 2014) pointed out that reducing the basis set used in the geometry and frequency calculation from 6 to 311++G(3df,3pd) to 6–31++G(d,p) contributes to a significant reduction in computational cost and only results in small errors in the thermal contribution to the Gibbs free energy and subsequent coupled cluster single point energy calculation, which indicates the rationality of choosing 6–31++G(d,p) as the basis set. The calculation of harmonic vibrational frequencies aimed to confirm that the obtained isomers were the true minima. Unless otherwise noted, thermochemical parameters were calculated using the rigid rotor-harmonic oscillator approximation (RRHO). The convergence criteria were under the default settings in the Gaussian 09 program package (Frisch et al., 2013). Here, only the lowest energy conformer was taken into consideration.

Single point energy calculations were performed at the theoretical level of DLPNO–CCSD(T)/aug–cc–pVTZ using the ORCA 4.0 suite of programs (Neese, 2012). The Gibbs free energy can be described by the equation below:

$$G_T = E_{sp} + TC_{G_T} \quad (1)$$

where E_{sp} is the absolute energy calculated at the DLPNO-CCSD(T)/aug–cc–pVTZ level of theory, and TC_{G_T} is the thermal correction to the Gibbs free energy at temperature T obtained at M06–2X/6–31++G (d,p). The calculations of enthalpy and zero-point corrected energy (ZPE) are similar to that of Gibbs free energy.

Subsequently, in order to clarify the nature of the hydrogen bond interactions in clusters of various sizes, the characteristics of the bond critical points (BCPs) were analyzed based on the atoms in molecules (AIM) (Bader, 1990) approach, which were performed in the Multiwfn program (Lu and Chen, 2012).

In order to evaluate the extent of proton transfer between acids and bases in cluster, the proton transfer parameter ρ_{PT} was used as a measure

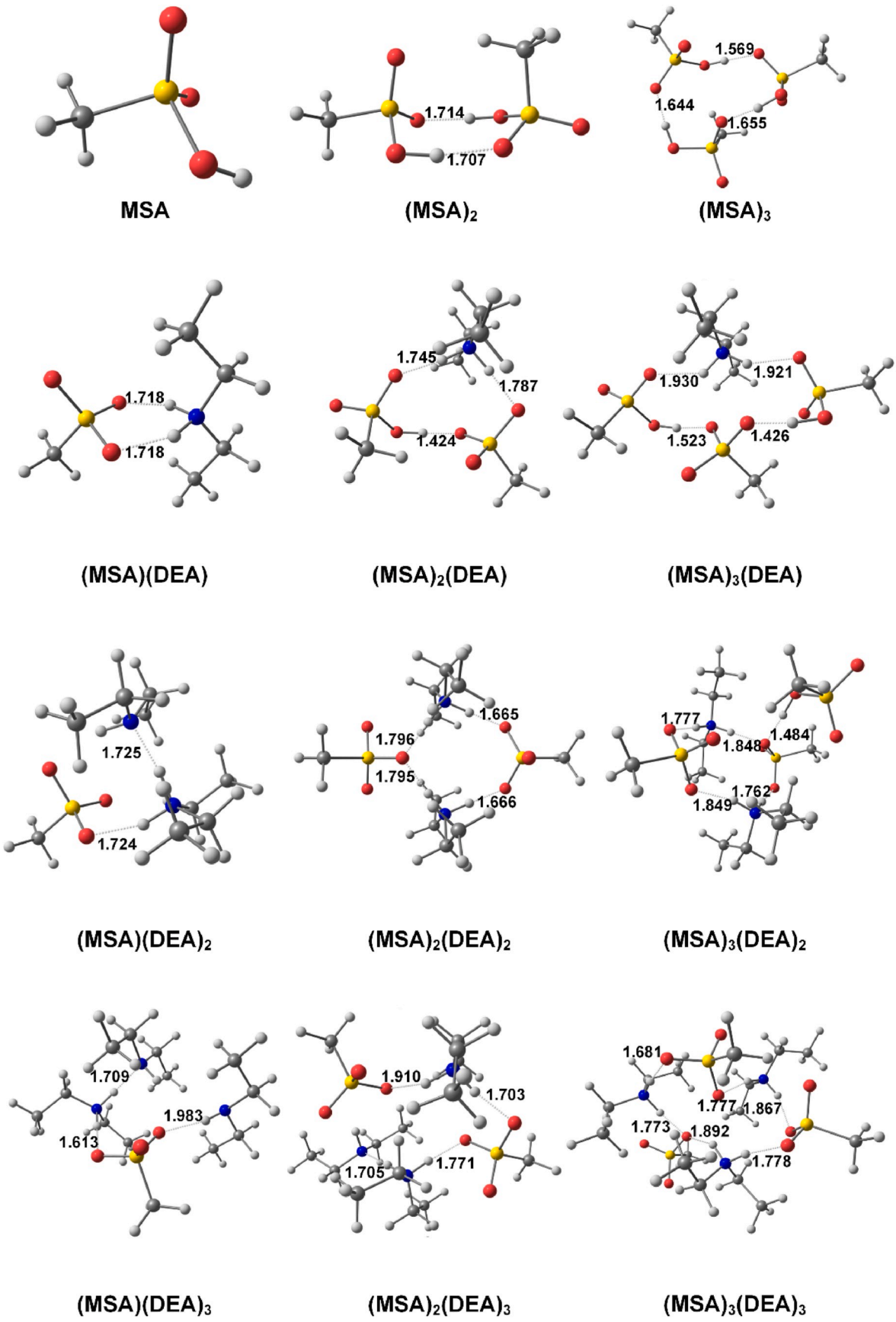

Fig. 1. Global minima of $(MSA)_m(DEA)_n$ $(m = 1-3$ and $n = 0-3)$ optimized at the M06–2X/6–31++G(d,p) level of theory.

of the extent of proton transfer, which evaluated the degree of ionization based on the inter atomic distances (Hunt et al., 2003; Kurnig and Scheiner, 1987). Here, the method to calculate the degree of proton transfer is based on the shortening of the NH bond and the elongation of the OH bond, as shown in equation (2):

$$\rho_{PT} = \left(r_{OH} - r^0_{OH}\right) - \left(r_{H\cdots N} - r^0_{H\cdots N}\right) \quad (2)$$

where r_{OH} and r^0_{OH} represent the length of the covalent OH bond of MSA in the cluster and in the monomer, respectively. $r_{H\cdots N}$ and $r^0_{H\cdots N}$ represent the length of H···N bond in the cluster and in the fully protonated diethylamine (DEA^+), respectively. For a cluster in which proton transfer has not occurred, the first term is nearly 0 and the second term is positive, so the proton transfer parameter ρ_{PT} is negative. When proton transfer occurs, the OH in the acid molecule will elongate, brings about a positive change in the first term, meanwhile, the amine in the cluster is completely protonated, making the second term close to 0, thus the proton transfer parameter is positive. (Hunt et al., 2003; Kurnig and Scheiner, 1987; Liu et al., 2018b)

The changes of Gibbs free energies ΔG_T were originally calculated at a reference pressure P_{ref} of 1 atm. Considering the effect of the actual vapor pressure during cluster formation, ΔG_T can be converted to the Gibbs free energy surface at the actual vapor pressure of the components (Olenius et al., 2013), named actual Gibbs free energy, as shown in equation (3):

$$\Delta G_a = \Delta G_T - k_B T \sum_{i=1}^{n} N_i \ln\left(\frac{P_i}{P_{ref}}\right) \quad (3)$$

where n is the number of components in the cluster, N_i is the number of molecules of type i in the cluster, P_i is the partial pressure of component i in the vapor phase, T is the temperature and k_B is the Boltzmann constant.

The formation rates of the clusters were obtained using dynamics simulation based on Atmospheric Cluster Dynamics Code (ACDC) solving the ordinary differential equations (McGrath et al., 2012). The formation rate simulation may be calculated by equation (4):

$$J = \sum_{i=1}^{3}\sum_{j=1}^{3}\sum_{k=0}^{3}\sum_{l=0}^{3}\beta_{ik,jl}c_{ik}c_{jl} \quad (4)$$

where i and j refer to the number of MSA molecules in the first and second cluster, k and l refer to the number of DEA molecules. Here, the formation rate given by equation (4) is not the nucleation rate, and therefore it is risky to directly compare the value of J reported here with the true nucleation rate. The time evolution of cluster concentration c_i can be obtained by solving the birth and death equation (McGrath et al., 2012) given by equation (5):

$$\frac{d_{c_i}}{dt} = \frac{1}{2}\sum_{j<i}\beta_{j,(i-j)}c_j c_{i-j} + \sum_j \gamma_{(i+j)\to i}c_{(i+j)} - \sum_j \beta_{i,j}c_i c_j - \frac{1}{2}\sum_{j<i}\gamma_{i\to j}c_i + Q_i - S_i \quad (5)$$

where Q_i refers to the additional source term of cluster i and S_i refers to the possible loss term for cluster i. $\beta_{i,j}$ represents the collision coefficient from kinetic theory (Ortega et al., 2012) and is calculated by equation (6):

$$\beta_{i,j} = \left(\frac{3}{4\pi}\right)^{1/6}\left(\frac{6k_bT}{m_i} + \frac{6k_bT}{m_j}\right)^{1/2}\left(V_i^{1/3} + V_j^{1/3}\right)^2 \quad (6)$$

where T represents the temperature, k_b represents the Boltzmann constant, and m_i and V_i represent the mass and volume of cluster i, respectively. The evaporation coefficient $\gamma_{(i+j)\to i}$ is calculated by equation (7):

$$\gamma_{(i+j)\to i,j} = \beta_{i,j}\frac{c_i^e c_j^e}{c_{i+j}^e} = \beta_{i,j}c_{ref}\exp\left(\frac{\Delta G_{i+j} - \Delta G_i - \Delta G_j}{k_b T}\right) \quad (7)$$

Where c_i^e corresponds to the equilibrium concentration of cluster i, and c_{ref} corresponds to the monomer concentration of the reference vapor. The simulation system is a "3 × 3 box" where 3 is the maximum number of acid or amine molecules in the cluster. Although smaller sizes may cause overestimation of formation rates, we are only focusing on the comparison of the formation rate of MSA-DEA with the results of SA-DMA and SA-MA systems of the same size and MSA-DMA cluster with a slightly different size. (Bork et al., 2014; Xie et al., 2017) The ACDC simulation was performed mainly at 278.15K. The condensation sink coefficient was set to a constant value of 2.6×10^{-3} s^{-1}, which corresponds to the typical values observed in the boreal forest environment. (Maso et al., 2008) The concentrations of MSA and SA were set at 10^5, 10^6, 10^7 and 10^8 cm^{-3}, which is the range associated with atmospheric NPF. (Eisele and Tanner, 1993; Berresheim et al., 2002) Liu et al. reported that the concentration of gaseous DEA at a mountain site in southern China ranges at ppt level. (Liu et al., 2018a) The study by Müller et al. (2009) also revealed a good correlation between DEA and DMA in the test samples. Therefore, the concentration of DEA was set at 0.1, 1 and 10 ppt, which corresponds to the typical concentration of DMA. (Olenius et al., 2013; Ge et al., 2011; Riipinen et al., 2007)

3. Results and discussion

3.1. Structural parameters

The global minimum structures of $(MSA)_m(DEA)_n$ ($m = 1-3$ and $n = 0-3$) are shown in Fig. 1. Detailed information on the lowest energy structures is enumerated in Table S2. As indicated in Fig. 1, significant hydrogen bonds are evident in the homomolecular clusters $(MSA)_m$, but no proton transfer occurred; thus, the stability of these clusters depends on the strength of the hydrogen bonds. However, in all heteromolecular clusters, both hydrogen bonds and proton transfer can be clearly observed. Therefore, not only the strength of hydrogen bonds, but also the strength of proton transfer, will affect the stability of these clusters.

Hydrogen bond is a significant intermolecular interaction in clusters (Kollman and Allen, 1972), so it's necessary to study the changes in the strength of hydrogen bonds in different clusters. In order to describe the strength of the hydrogen bonds as the cluster size increases, the topological parameters of homomolecular clusters $(MSA)_m$ ($m = 2-3$) are discussed. Table S3 lists the partial parameters in the $(MSA)_m$ ($m = 2-3$) topological analysis, including the electron density (ρ), its Laplacian ($\nabla^2\rho$), and the electronic energy density (E), which is made up of the electronic kinetic energy density (G) and the electronic potential energy density (V). Larger electron density values correspond to stronger hydrogen bonds (Bader, 1990). When both $\nabla^2\rho$ and E are greater than 0, it corresponds to a weak hydrogen bond. A case where $\nabla^2\rho$ is positive and E is negative represents a medium hydrogen bond. If both $\nabla^2\rho$ and E are all negative, this case corresponds to a strong hydrogen bond (Rozas et al., 2000). As can be seen in Table S3, in the homomolecular clusters, as the number of MSA molecules increases from 2 to 3, more hydrogen bonds with larger electron density values are generated, in other words, the intensities of the hydrogen bonds in the clusters are enhanced.

Proton transfer plays an important role in cluster stability (Stinson et al., 2016). As can be seen in Table S4, in all heteromolecular clusters, due to the strength of the acid and the base, proton transfer occurs generally. Proton transfer parameters were used to assess whether proton transfer occurred in the hydrogen bonds within the cluster. A positive value of ρ_{PT} suggests a fully transferred proton interaction and a negative value of ρ_{PT} corresponds to the ordinary hydrogen bond. As shown in Table S4, for the $(MSA)_m(DEA)_n$ ($m = 1-3$ and $n = 1-3$) clusters, all the proton transfer parameters are positive, which indicates

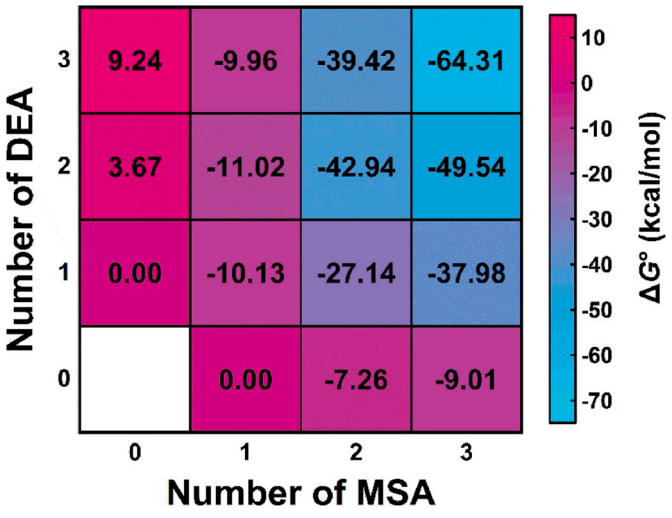

Fig. 2. Standard Gibbs free energies changes for $(MSA)_m(DEA)_n$ ($m = 0-3$ and $n = 0-3$) clusters at the DLPNO–CCSD(T)/aug–cc–pVTZ//M06–2X/6–31++G(d,p) level and at 298.15 K and 1 atm.

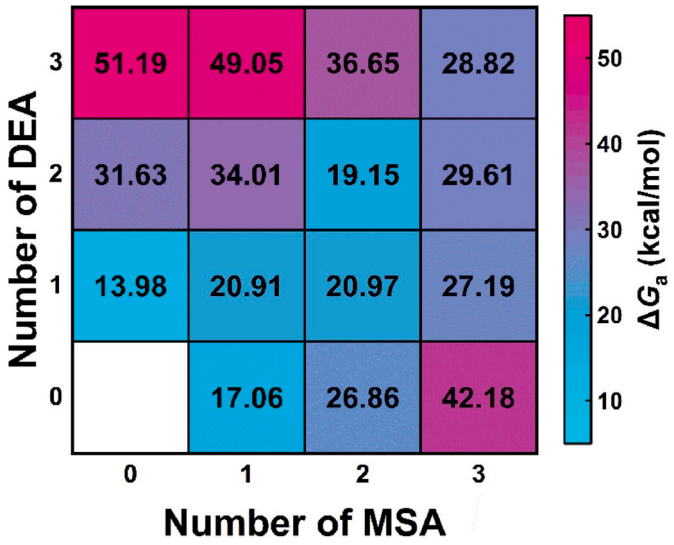

Fig. 3. Actual Gibbs free energy surfaces of $(MSA)_m(DEA)_n$ ($m = 0-3$ and $n = 0-3$) clusters, at 278.15 K, [MSA] = 10^6 cm^{-3}, [DEA] = 10 ppt.

that proton transfer generally occurs in these clusters. When $m = n$, the amine (–NH) groups of all DEA molecules are protonated by MSA, while each MSA molecule transfers a single proton to form a cyclic structure between MSA and DEA. When $m \neq n$, the number of proton transfers depends on the smaller value in m or n. Since MSA can only provide one proton and DEA can only accept one proton, the number of proton transfers is limited by the number of acid-base pairs. As shown in Fig. 1, when the number of acids and bases is the same, such as $(MSA)_2(DEA)_2$ and $(MSA)_3(DEA)_3$, it is obvious that each MSA molecule is connected to two DEA molecules and each DEA molecule is connected to two MSA molecules, forming an acid-base cyclic structure. For each DEA molecule, its original H atom is connected to an MSA molecule by a hydrogen bond. When connected to another MSA molecule, the H atom from proton transfer is used.

3.2. Thermodynamics analysis

The thermodynamic parameter, especially the standard Gibbs free energy, is a parameter that can effectively reveal the stability of a cluster. The standard Gibbs free energies changes associated with the different sizes of the MSA–DEA clusters are presented in Fig. 2, and the corresponding thermodynamic quantities ΔE_0, ΔH and ΔS are presented in Table S5. Here, the effect of multiple conformers on Gibbs free energies was ignored, and only the lowest energy conformer was treated. According to Partanen et al. (2016), because of the logarithmic dependence on free energies in the correct free-energy formulas, only a few molecules or clusters contribute to the free energy. At the same time, the difference in Gibbs free energy between different isomers may exceed 10 kcal/mol, so it's important to find the lowest energy comforter. As can be seen in Fig. 2, the standard Gibbs free energy changes of the acid-base clusters are invariably negative, which demonstrates that the reactions forming these clusters are spontaneous.

The standard Gibbs free energy change of (MSA)(DEA) is 2.87 kcal/mol more negative than that of $(MSA)_2$ as shown in Fig. 2, which indicates that when the cluster contains two molecules, proton transfer occurs in the heteromolecular clusters, which introduces factors that enhance the stability of the clusters. In addition, it can be observed that the ΔG° values of the diagonal clusters are more negative. This is related to the number of transferable protons in the cluster. As the number of acids and bases increases from 1 to 3, the ΔG° value of the cluster changes from −10.13 kcal/mol to −64.31 kcal/mol. A more negative free energy favors cluster formation and indicates cluster stability, which may contribute to cluster growth to a detectable particle size.

3.3. Thermodynamics at ambient concentration: actual free energy

In the actual analysis of atmospheric NPF, apart from the thermodynamic parameters of the clusters, it is also necessary to consider the free energy surface of the cluster under certain conditions. The free energy surface of the cluster is the actual Gibbs free energy at the given monomer vapor pressure, which describes the Gibbs free energy barrier in the cluster growth (Olenius et al., 2013). The Gibbs free energy surfaces of the MSA–DEA clusters calculated at ambient trace gas concentrations are shown in Fig. 3. The concentration of MSA was set to [MSA] = 10^6 molecules cm^{-3}, and the mixing ratio of DEA was set to 10 ppt. All calculations were performed at 278.15 K.

As shown in Fig. 3, along the diagonal on the acid-base grid, the free energy surfaces appear to be lowest. For the $(MSA)_2(DEA)_2$ and $(MSA)_3(DEA)_3$ clusters in particular, the free energy surfaces are 18.99 and 28.57 kcal/mol, respectively, which is lower than other clusters with similar sizes. A similar trend of low free energy barriers along the diagonal was revealed in the SA-DMA/SA-NH_3 systems by Olenius et al. (2013) In addition, the free energy surfaces of clusters with one more base than an acid molecule are much higher than that of clusters with one more acid than a base molecule. The main reason for this phenomenon is that clusters with more acid molecules can form a ring structure, but no ring structure is observed on clusters with more base molecules, and at the same time, more and stronger hydrogen bonds are formed between the acid–acid molecules and the acid–base molecules. These all contribute to the stability of these clusters.

3.4. Evaporation rates

Regarding the formation of acid-base clusters and its atmospheric significance, the evaporation rate and collision coefficient affect the stability of the cluster where non-monomers collide and evaporate from clusters just like monomers (Ortega et al., 2012; Arstila, 1997; Vehkamäki et al., 2012). For the MSA–DEA system, the collision coefficients of the clusters differ little; therefore, the differences in evaporation rate reveal the stability of the cluster at a given acid and base concentration. The evaporation rates for $(MSA)_m(DEA)_n$ ($m = 0-3$ and $n = 0-3$) on the MSA–DEA grid at 278.15 K are presented in Fig. 4. Clusters with smaller evaporation rates are less likely to evaporate and form small

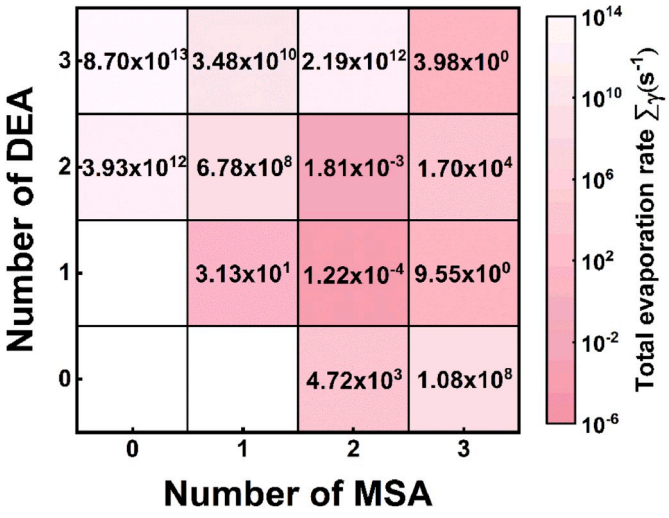

Fig. 4. Evaporation rates for $(MSA)_m(DEA)_n$ $(m = 0-3$ and $n = 0-3)$ on the MSA–DEA grid at 278.15 K.

clusters. In the process of acid-base cluster growth, considering the collision with acid, base monomer, or other cluster, a cluster with a higher collision rate than its own evaporation rate can be considered as a stable cluster (Xie et al., 2017). In general, the collision rate constant of a cluster with acid or base is of the order of 10^{-10} cm^3 s^{-1}. When the concentration of acid or base monomer is at several ppt, the collision rate of the cluster with acid or base monomer reaches about 10^{-1} s^{-1}. Therefore, clusters with an evaporation rate lower than 10^{-1} s^{-1} may be considered as stable clusters. Among most evaporation pathways (see Table S6), the main evaporation route is the evaporation of MSA or DEA monomer from the cluster, rather than evaporation of the dimer cluster as reported by McGrath et al. (2012) This is mainly because the Gibbs free energy surface of the dimer of SA and DMA is smaller than that of the monomer, which corresponds to stronger stability of the dimer, while the situation of MSA and DEA is opposite. When the number of acids and bases in the cluster is unequal, for example, the number of acids is greater than that of bases, the evaporation of the acid monomer from the cluster will be apparent. When two clusters share the same number of molecules, the total evaporation rate of the cluster with more amine molecules is higher than that of clusters with more acid molecules. This is a manifestation of the stronger bonding capability of MSA with clusters than that of DEA.

3.5. New particle formation rates

Cluster formation rate can be used as an important indicator to characterize the stabilization of acid and base NPF (Almeida et al., 2013; McGrath et al., 2012; Xie et al., 2017; Olenius et al., 2017; Jen et al., 2014). Experimental evidence has shown that SA–DMA and SA–methylamine (MA) systems at the ppt level have the potential for NPF (Almeida et al., 2013; Jen et al., 2014). Chen et al. (2015b) pointed out that MSA–DMA plays an important role in driving NPF. To verify the nucleation potential of MSA and DEA, the simulated formation rate of the MSA–DEA system was compared with that of SA–DMA and SA–MA systems of the same cluster size (3 × 3 box) (Xie et al., 2017) and that of MSA–DMA system of a slightly different size (3 × 2 box) (Bork et al., 2014). Considering that the most appropriate functional for describing the geometric and thermodynamic properties of each cluster is different, the thermodynamic parameters of each cluster were obtained by using their most suitable functional. Other simulation conditions are the same.

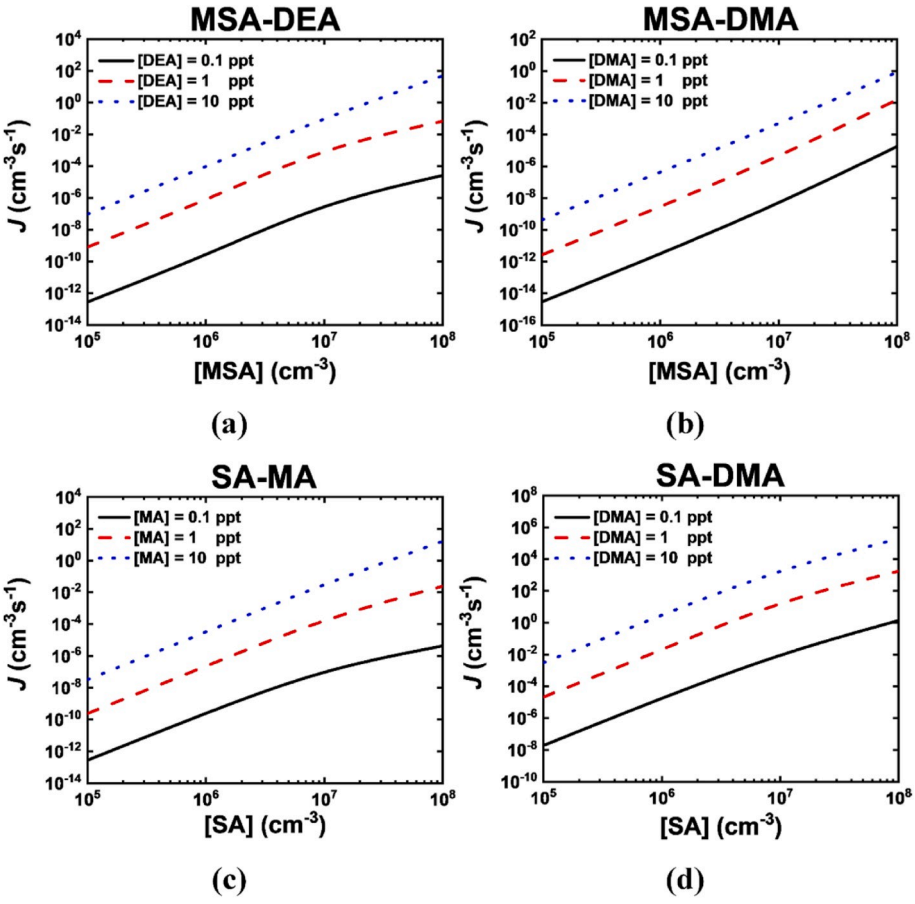

Fig. 5. The cluster formation rate J (cm^{-3} s^{-1}) as a function of acid monomer concentration for different systems: (a) MSA-DEA, (b) MSA-DMA, (c) SA-MA, (d) SA-DMA. The black solid lines represent [base] = 0.1 ppt, the red dashed lines represent [base] = 1 ppt and the blue dotted lines represent [base] = 10 ppt. All simulations were performed at 278.15 K and 1 atm. (For interpretation of the references to colour in this figure legend, the reader is referred to the Web version of this article.)

The cluster formation rate as a function of acid monomer concentration at 278.15 K is shown in Fig. 5. More importantly, for the same cluster size, when sharing the same precursor concentration, the formation rate of the MSA–DEA system was 10^1–10^3 times that of the MSA–DMA system, 1–6 times that of the SA–MA system, and 10^{-4}–10^{-5} times that of the SA–DMA system. It can be expected that the MSA-DEA system has a strong ability of new particle formation, which is between SA-DMA and SA-MA system. However, MSA–DEA has a higher formation rate than MSA–DMA, corresponding to the more negative Gibbs free energies between MSA and DEA. When comparing the dimers of the MSA-DMA system and the MSA-DEA system, we found that MSA and DEA formed a stable planar cyclic structure, while MSA and DMA did not form a similar ring structure.

The SA–DMA and the SA–MA systems at the ppt level have been shown to promote atmospheric NPF (Almeida et al., 2013; Jen et al., 2014). Therefore, it can be concluded that the MSA–DEA system can enhance NPF when the atmospheric concentration of DEA and MSA reaches the ppt level.

4. Conclusions

In this study, the strong aerosol formation capabilities of DEA when interacting with MSA have been demonstrated using cluster kinetic modelling. The results agree well with the high-particulate DEA concentrations observed in field studies in the marine environment. Specifically, by comparing the formation rates of the MSA–DEA system with several other systems of the same size, it was shown that the nucleation potential of the MSA–DEA system is inferior to that of sulfuric acid (SA)–DMA, and slightly superior to that of SA–methylamine (MA) but superior to that of MSA–DMA. The mechanism of NPF has been studied systematically and in some detail: structural and thermodynamic results indicate a tendency for clusters to be stable for increasing cluster size. Furthermore, combining the diagonal distribution of lower free energy clusters and the number of proton transfers, the influence of proton transfer on cluster growth is revealed. In view of the low evaporation rate, clusters near the diagonal can be considered stable. In addition, the evaporation rate of clusters containing amine molecules is greater than that of clusters with acid groups, indicating that MSA has a stronger binding capability than DEA.

Studies of the influence of hydration on NPF in the SA/ammonia and SA/DMA systems show that the effect of hydration on NPF in the system diminishes with increasing nucleation ability of the binary acid-base system (Henschel et al., 2016). Therefore, it is reasonable to assume that the role of water in the MSA–DEA system is weaker than in the MSA–DMA system. However, the specific impact of hydration on the MSA–DEA system still needs further investigation.

Declaration of competing interest

The authors declare that they have no known competing financial interests or personal relationships that could have appeared to influence the work reported in this paper.

CRediT authorship contribution statement

Cai-Xin Xu: Conceptualization, Methodology, Data curation, Writing - original draft, Writing - review & editing. **Shuai Jiang:** Methodology, Validation, Formal analysis, Writing - review & editing. **Yi-Rong Liu:** Software, Investigation, Visualization. **Ya-Juan Feng:** Formal analysis, Data curation. **Zi-Hang Wang:** Writing - review & editing. **Teng Huang:** Resources. **Yu Zhao:** Visualization. **Jie Li:** Visualization. **Wei Huang:** Methodology, Software, Supervision, Project administration, Funding acquisition.

Acknowledgements

This work was supported by the National Natural Science Foundation of China (Grant No. 41877305, 21573241, 41605099, 41705097, 41705111, 41775112 and 41527808), the National Science Fund for Distinguished Young Scholars (Grant No. 41725019), Key Research Program of Frontier Science, CAS (Grant No. QYZDB-SSW-DQC031), The Key Research Program of the Chinese Academy of Sciences (Grant No. ZDRW-ZS-2016-4-3-6), the National Key Research and Development program (Grant No. 2016YFC0202203), National Research Program for Key Issues in Air Pollution Control (DQGG0103) and the Fundamental Research Funds for the Central Universities (Grant No. WK2100100031).

Appendix A. Supplementary data

Supplementary data to this article can be found online at https://doi.org/10.1016/j.atmosenv.2020.117404.

References

Aalto, P., Hämeri, K., Becker, E., Weber, R., Salm, J., Mäkelä, J.M., Hoell, C., O'dowd, C. D., Hansson, H.-C., Väkevä, M., 2001. Physical characterization of aerosol particles during nucleation events. Tellus B 53 (4), 344–358.

Almeida, J., Schobesberger, S., Kürten, A., Ortega, I.K., Kupiainen-Määttä, O., Praplan, A. P., Adamov, A., Amorim, A., Bianchi, F., Breitenlechner, M., 2013. Molecular understanding of sulphuric acid–amine particle nucleation in the atmosphere. Nature 502 (7471), 359.

Arstila, H., 1997. Kinetic effect of cluster-cluster processes on homogeneous nucleation rates in one-and two-component systems. J. Chem. Phys. 107 (8), 3196–3203.

Bader, R., 1990. Atoms in Molecule:A Quantum Theory. Clarendon, Oxford, UK.

Bates, T., Lamb, B., Guenther, A., Dignon, J., Stoiber, R., 1992. Sulfur emissions to the atmosphere from natural sources. J. Atmos. Chem. 14 (1–4), 315–337.

Berndt, T., Böge, O., Stratmann, F., Heintzenberg, J., Kulmala, M., 2005. Rapid formation of sulfuric acid particles at near-atmospheric conditions. Science 307 (5710), 698–700.

Berresheim, H., Elste, T., Tremmel, H.G., Allen, A.G., Hansson, H.C., Rosman, K., Dal Maso, M., Mäkelä, J.M., Kulmala, M., O'Dowd, C.D., 2002. Gas-aerosol relationships of H_2SO_4, MSA, and OH: observations in the coastal marine boundary layer at Mace Head, Ireland. J. Geophys. Res. Atmos. 107 (D19), 8100.

Bork, N., Elm, J., Olenius, T., Vehkamäki, H., 2014. Methane sulfonic acid-enhanced formation of molecular clusters of sulfuric acid and dimethyl amine. Atmos. Chem. Phys. 14 (22), 12023–12030.

Brus, D., Hyvärinen, A.-P., Viisanen, Y., Kulmala, M., Lihavainen, H., 2010. Homogeneous nucleation of sulfuric acid and water mixture: experimental setup and first results. Atmos. Chem. Phys. 10 (6), 2631–2641.

Charlson, R.J., Seinfeld, J.H., Nenes, A., Kulmala, M., Laaksonen, A., Facchini, M.C., 2001. Reshaping the theory of cloud formation. Science 292 (5524), 2025–2026.

Chen, H., Finlayson-Pitts, B.J., 2016. New particle formation from methanesulfonic acid and amines/ammonia as a function of temperature. Environ. Sci. Technol. 51 (1), 243–252.

Chen, H., Ezell, M.J., Arquero, K.D., Varner, M.E., Dawson, M.L., Gerber, R.B., Finlayson-Pitts, B.J., 2015a. New particle formation and growth from methanesulfonic acid, trimethylamine and water. Phys. Chem. Chem. Phys. 17 (20), 13699–13709.

Chen, H., Varner, M.E., Gerber, R.B., Finlayson-Pitts, B.J., 2015b. Reactions of methanesulfonic acid with amines and ammonia as a source of new particles in air. J. Phys. Chem. B 120 (8), 1526–1536.

Dawson, M.L., Varner, M.E., Perraud, V., Ezell, M.J., Gerber, R.B., Finlayson-Pitts, B.J., 2012. Simplified mechanism for new particle formation from methanesulfonic acid, amines, and water via experiments and ab initio calculations. Proc. Natl. Acad. Sci. U.S.A. 109 (46), 18719–18724.

Eisele, F., Tanner, D., 1993. Measurement of the gas phase concentration of H_2SO_4 and methane sulfonic acid and estimates of H_2SO_4 production and loss in the atmosphere. J. Geophys. Res. Atmos. 98 (D5), 9001–9010.

Elm, J., Kristensen, K., 2017. Basis set convergence of the binding energies of strongly hydrogen-bonded atmospheric clusters. Phys. Chem. Chem. Phys. 19 (2), 1122–1133.

Elm, J., Mikkelsen, K.V., 2014. Computational approaches for efficiently modelling of small atmospheric clusters. Chem. Phys. Lett. 615, 26–29.

Elm, J., Bilde, M., Mikkelsen, K.V., 2012. Assessment of density functional theory in predicting structures and free energies of reaction of atmospheric prenucleation clusters. J. Chem. Theor. Comput. 8 (6), 2071–2077.

Elm, J., Fard, M., Bilde, M., Mikkelsen, K.V., 2013. Interaction of glycine with common atmospheric nucleation precursors. J. Phys. Chem. A 117 (48), 12990–12997.

Elm, J., Jen, C.N., Kurtén, T., Vehkamäki, H., 2016. Strong hydrogen bonded molecular interactions between atmospheric diamines and sulfuric acid. J. Phys. Chem. A 120 (20), 3693–3700.

Elm, J., Myllys, N., Olenius, T., Halonen, R., Kurtén, T., Vehkamäki, H., 2017. Formation of atmospheric molecular clusters consisting of sulfuric acid and C 8 H 12 O 6 tricarboxylic acid. Phys. Chem. Chem. Phys. 19 (6), 4877–4886.

Ezell, M.J., Chen, H., Arquero, K.D., Finlayson-Pitts, B.J., 2014. Aerosol fast flow reactor for laboratory studies of new particle formation. J. Aerosol Sci. 78, 30–40.
Facchini, M.C., Decesari, S., Rinaldi, M., Carbone, C., Finessi, E., Mircea, M., Fuzzi, S., Moretti, F., Tagliavini, E., Ceburnis, D., 2008. Important source of marine secondary organic aerosol from biogenic amines. Environ. Sci. Technol. 42 (24), 9116–9121.
Fitzgerald, J.W., 1991. Marine aerosols: a review. Atmos. Environ. 25 (3–4), 533–545.
Frisch, M., Trucks, G., Schlegel, H., Scuseria, G., Robb, M., Cheeseman, J., Scalmani, G., Barone, V., Mennucci, B., Petersson, G., 2013. Gaussian 09, Revision D. 01, 2013, Gaussian. Gaussian Inc., Wallingford CT.
Gaston, C.J., Pratt, K.A., Qin, X., Prather, K.A., 2010. Real-time detection and mixing state of methanesulfonate in single particles at an inland urban location during a phytoplankton bloom. Environ. Sci. Technol. 44 (5), 1566–1572.
Ge, X., Wexler, A.S., Clegg, S.L., 2011. Atmospheric amines–Part I. A review. Atmos. Environ. 45 (3), 524–546.
Hanson, D., 2005. Mass accommodation of H_2SO_4 and CH_3SO_3H on Water– sulfuric acid solutions from 6% to 97% RH. J. Phys. Chem. A 109 (31), 6919–6927.
Henschel, H., Navarro, J.C.A., Yli-Juuti, T., Kupiainen-Määttä, O., Olenius, T., Ortega, I. K., Clegg, S.L., Kurtén, T., Riipinen, I., Vehkamäki, H., 2014. Hydration of atmospherically relevant molecular clusters: computational chemistry and classical thermodynamics. J. Phys. Chem. A 118 (14), 2599–2611.
Henschel, H., Kurtén, T., Vehkamäki, H., 2016. Computational study on the effect of hydration on new particle formation in the sulfuric acid/ammonia and sulfuric acid/dimethylamine systems. J. Phys. Chem. A 120 (11), 1886–1896.
Hinds, W.C., 2012. Aerosol Technology: Properties, Behavior, and Measurement of Airborne Particles. John Wiley & Sons.
Hopkins, R.J., Desyaterik, Y., Tivanski, A.V., Zaveri, R.A., Berkowitz, C.M., Tyliszczak, T., Gilles, M.K., Laskin, A., 2008. Chemical speciation of sulfur in marine cloud droplets and particles: analysis of individual particles from the marine boundary layer over the California current. J. Geophys. Res. Atmos. 113 (D4), D04209.
Hostaš, J., Řezáč, J., Hobza, P., 2013. On the performance of the semiempirical quantum mechanical PM6 and PM7 methods for noncovalent interactions. Chem. Phys. Lett. 568, 161–166.
Huang, W., Pal, R., Wang, L.-M., Zeng, X.C., Wang, L.-S., 2010. Isomer identification and resolution in small gold clusters. J. Chem. Phys. 132 (5), 054305.
Hunt, S.W., Higgins, K.J., Craddock, M.B., Brauer, C.S., Leopold, K.R., 2003. Influence of a polar near-neighbor on incipient proton transfer in a strongly hydrogen bonded complex. J. Am. Chem. Soc. 125 (45), 13850–13860.
Jen, C.N., McMurry, P.H., Hanson, D.R., 2014. Stabilization of sulfuric acid dimers by ammonia, methylamine, dimethylamine, and trimethylamine. J. Geophys. Res. Atmos. 119 (12), 7502–7514.
Jiang, S., Liu, Y.-R., Huang, T., Wen, H., Xu, K.-M., Zhao, W.-X., Zhang, W.-J., Huang, W., 2014. Study of Cl-(H2O)n (n= 1–4) using basin-hopping method coupled with density functional theory. J. Comput. Chem. 35 (2), 159–165.
Kirkby, J., Duplissy, J., Sengupta, K., Frege, C., Gordon, H., Williamson, C., Heinritzi, M., Simon, M., Yan, C., Almeida, J., 2016. Ion-induced nucleation of pure biogenic particles. Nature 533 (7604), 521.
Kollman, P.A., Allen, L.C., 1972. Theory of the hydrogen bond. Chem. Rev. 72 (3), 283–303.
Kreidenweis, S.M., Seinfeld, J.H., 1967. Nucleation of sulfuric acid-water and methanesulfonic acid-water solution particles: implications for the atmospheric chemistry of organosulfur species. Atmos. Environ. 22 (2), 283–296, 1988.
Kulmala, M., 2003. How particles nucleate and grow. Science 302 (5647), 1000–1001.
Kulmala, M., Petäjä, T., Nieminen, T., Sipilä, M., Manninen, H.E., Lehtipalo, K., Dal Maso, M., Aalto, P.P., Junninen, H., Paasonen, P., 2012. Measurement of the nucleation of atmospheric aerosol particles. Nat. Protoc. 7 (9), 1651.
Kupiainen, O., Ortega, I., Kurtén, T., Vehkamäki, H., 2012. Amine substitution into sulfuric acid–ammonia clusters. Atmos. Chem. Phys. 12 (8), 3591–3599.
Kurnig, I.J., Scheiner, S., 1987. Ab Initio investigation of the structure of hydrogen halide-amine complexes in the gas phase and in a polarizable medium. Int. J. Quant. Chem. 32 (S14), 47–56.
Kurtén, T., Loukonen, V., Vehkamäki, H., Kulmala, M., 2008. Amines are likely to enhance neutral and ion-induced sulfuric acid-water nucleation in the atmosphere more effectively than ammonia. Atmos. Chem. Phys. 8 (14), 4095–4103.
Kürten, A., Münch, S., Rondo, L., Bianchi, F., Duplissy, J., Jokinen, T., Junninen, H., Sarnela, N., Schobesberger, S., Simon, M., 2015. Thermodynamics of the formation of sulfuric acid dimers in the binary (H_2SO_4–H_2O) and ternary (H_2SO_4–H_2O–NH_3) system. Atmos. Chem. Phys. 15 (18), 10701–10721.
Li, S., Zhang, L., Qin, W., Tao, F.-M., 2007. Intermolecular structure and properties of the methanesulfonic acid–ammonia system in small water clusters. Chem. Phys. Lett. 447 (1–3), 33–38.
Liu, Y.-R., Wen, H., Huang, T., Lin, X.-X., Gai, Y.-B., Hu, G.-J., Zhang, W.-J., Huang, W., 2014. Structural exploration of water, nitrate/water, and oxalate/water clusters with basin-hopping method using a compressed sampling technique. J. Phys. Chem. A 118 (2), 508–516.
Liu, F., Bi, X., Zhang, G., Peng, L., Lian, X., Lu, H., Fu, Y., Wang, X., Peng, P.a., Sheng, G., 2017. Concentration, size distribution and dry deposition of amines in atmospheric particles of urban Guangzhou, China. Atmos. Environ. 171, 279–288.
Liu, F., Bi, X., Zhang, G., Lian, X., Fu, Y., Yang, Y., Lin, Q., Jiang, F., Wang, X., Peng, P.a., 2018a. Gas-to-particle partitioning of atmospheric amines observed at a mountain site in southern China. Atmos. Environ. 195, 1–11.
Liu, L., Li, H., Zhang, H., Zhong, J., Bai, Y., Ge, M., Li, Z., Chen, Y., Zhang, X., 2018b. The role of nitric acid in atmospheric new particle formation. Phys. Chem. Chem. Phys. 20 (25), 17406–17414.
Loukonen, V., Kurtén, T., Ortega, I., Vehkamäki, H., Padua, A.A., Sellegri, K., Kulmala, M., 2010. Enhancing effect of dimethylamine in sulfuric acid nucleation in the presence of water–a computational study. Atmos. Chem. Phys. 10 (10), 4961–4974.
Lu, T., Chen, F., 2012. Multiwfn: a multifunctional wavefunction analyzer. J. Comput. Chem. 33 (5), 580–592.
Maia, J.D.C., Urquiza Carvalho, G.A., Mangueira Jr., C.P., Santana, S.R., Cabral, L.A.F., Rocha, G.B., 2012. GPU linear algebra libraries and GPGPU programming for accelerating MOPAC semiempirical quantum chemistry calculations. J. Chem. Theor. Comput. 8 (9), 3072–3081.
Maso, M.D., Hyvaerinen, A., Komppula, M., Tunved, P., Kerminen, V.-M., Lihavainen, H., Viisanen, Y., Hansson, H.-C., Kulmala, M., 2008. Annual and interannual variation in boreal forest aerosol particle number and volume concentration and their connection to particle formation. Tellus B 60 (4), 495–508.
McGrath, M., Olenius, T., Ortega, I., Loukonen, V., Paasonen, P., Kurtén, T., Kulmala, M., Vehkamäki, H., 2012. Atmospheric Cluster Dynamics Code: a flexible method for solution of the birth-death equations. Atmos. Chem. Phys. 12 (5), 2345–2355.
Meinardi, S., Simpson, I.J., Blake, N.J., Blake, D.R., Rowland, F.S., 2003. Dimethyl disulfide (DMDS) and dimethyl sulfide (DMS) emissions from biomass burning in Australia. Geophys. Res. Lett. 30 (9), 1454.
Müller, C., Iinuma, Y., Karstensen, J., Pinxteren, D.v., Lehmann, S., Gnauk, T., Herrmann, H., 2009. Seasonal variation of aliphatic amines in marine sub-micrometer particles at the Cape Verde islands. Atmos. Chem. Phys. 9 (24), 9587–9597.
Muñiz-Unamunzaga, M., Borge, R., Sarwar, G., Gantt, B., de la Paz, D., Cuevas, C.A., Saiz-Lopez, A., 2018. The influence of ocean halogen and sulfur emissions in the air quality of a coastal megacity: the case of Los Angeles. Sci. Total Environ. 610, 1536–1545.
Nadykto, A., Yu, F., Jakovleva, M., Herb, J., Xu, Y., 2011. Amines in the Earth's atmosphere: a density functional theory study of the thermochemistry of pre-nucleation clusters. Entropy 13 (2), 554–569.
Nadykto, A.B., Herb, J., Yu, F., Xu, Y., 2014. Enhancement in the production of nucleating clusters due to dimethylamine and large uncertainties in the thermochemistry of amine-enhanced nucleation. Chem. Phys. Lett. 609, 42–49.
Nadykto, A., Herb, J., Yu, F., Xu, Y., Nazarenko, E., 2015. Estimating the lower limit of the impact of amines on nucleation in the Earth's atmosphere. Entropy 17 (5), 2764–2780.
Napari, I., Kulmala, M., Vehkamäki, H., 2002. Ternary nucleation of inorganic acids, ammonia, and water. J. Chem. Phys. 117 (18), 8418–8425.
Neese, F., 2012. The ORCA program system. WIREs Comput. Mol. Sci. 2 (1), 73–78.
Olenius, T., Kupiainen-Määttä, O., Ortega, I., Kurtén, T., Vehkamäki, H., 2013. Free energy barrier in the growth of sulfuric acid–ammonia and sulfuric acid–dimethylamine clusters. J. Chem. Phys. 139 (8), 084312.
Olenius, T., Halonen, R., Kurtén, T., Henschel, H., Kupiainen-Määttä, O., Ortega, I.K., Jen, C.N., Vehkamäki, H., Riipinen, I., 2017. New particle formation from sulfuric acid and amines: comparison of monomethylamine, dimethylamine, and trimethylamine. J. Geophys. Res. Atmos. 122 (13), 7103–7118.
Ortega, I., Kupiainen, O., Kurtén, T., Olenius, T., Wilkman, O., McGrath, M., Loukonen, V., Vehkamäki, H., 2012. From quantum chemical formation free energies to evaporation rates. Atmos. Chem. Phys. 12 (1), 225–235.
Palve, S., Nemade, P., Ghude, S., 2018. Effect of aerosols on ocean parameters in India by using satellite data. Procedia Comput. Sci. 132, 1857–1865.
Partanen, L., Vehkamäki, H., Hansen, K., Elm, J., Henschel, H., Kurtén, T., Halonen, R., Zapadinsky, E., 2016. Effect of conformers on free energies of atmospheric complexes. J. Phys. Chem. A 120 (43), 8613–8624.
Paytan, A., Mackey, K.R., Chen, Y., Lima, I.D., Doney, S.C., Mahowald, N., Labiosa, R., Post, A.F., 2009. Toxicity of atmospheric aerosols on marine phytoplankton. Proc. Natl. Acad. Sci. U.S.A. 106 (12), 4601–4605.
Perraud, V., Horne, J.R., Martinez, A.S., Kalinowski, J., Meinardi, S., Dawson, M.L., Wingen, L.M., Dabdub, D., Blake, D.R., Gerber, R.B., 2015. The future of airborne sulfur-containing particles in the absence of fossil fuel sulfur dioxide emissions. Proc. Natl. Acad. Sci. U.S.A. 112 (44), 13514–13519.
Riipinen, I., Sihto, S.-L., Kulmala, M., Arnold, F., Maso, M.D., Birmili, W., Saarnio, K., Teinilä, K., Kerminen, V.-M., Laaksonen, A., 2007. Connections between atmospheric sulphuric acid and new particle formation during QUEST III–IV campaigns in Heidelberg and Hyytiälä. Atmos. Chem. Phys. 7 (8), 1899–1914.
Rinaldi, M., Decesari, S., Finessi, E., Giulianelli, L., Carbone, C., Fuzzi, S., O'Dowd, C.D., Ceburnis, D., Facchini, M.C., 2010. Primary and secondary organic marine aerosol and oceanic biological activity: recent results and new perspectives for future studies. Adv. Meteorol. 2010, 310682.
Rosenfeld, P.E., Henry, C.L., Dills, R.L., Harrison, R.B., 2001. Comparison of odor emissions from three different biosolids applied to forest soil. Water, Air. Soil Pollut. 127 (1–4), 173–191.
Rozas, I., Alkorta, I., Elguero, J., 2000. Behavior of ylides containing N, O, and C atoms as hydrogen bond acceptors. J. Am. Chem. Soc. 122 (45), 11154–11161.
Sipilä, M., Berndt, T., Petäjä, T., Brus, D., Vanhanen, J., Stratmann, F., Patokoski, J., Mauldin, R.L., Hyvärinen, A.-P., Lihavainen, H., 2010. The role of sulfuric acid in atmospheric nucleation. Science 327 (5970), 1243–1246.
Sorooshian, A., Padró, L.T., Nenes, A., Feingold, G., McComiskey, A., Hersey, S.P., Gates, H., Jonsson, H.H., Miller, S.D., Stephens, G.L., 2009. On the link between ocean biota emissions, aerosol, and maritime clouds: airborne, ground, and satellite measurements off the coast of California. Global Biogeochem. Cycles 23 (4), GB4007.
Stinson, J.L., Kathmann, S.M., Ford, I.J., 2016. A classical reactive potential for molecular clusters of sulphuric acid and water. Mol. Phys. 114 (2), 172–185.
Temelso, B., Morrell, T.E., Shields, R.M., Allodi, M.A., Wood, E.K., Kirschner, K.N., Castonguay, T.C., Archer, K.A., Shields, G.C., 2012. Quantum mechanical study of

sulfuric acid hydration: atmospheric implications. J. Phys. Chem. A 116 (9), 2209–2224.
Tröstl, J., Chuang, W.K., Gordon, H., Heinritzi, M., Yan, C., Molteni, U., Ahlm, L., Frege, C., Bianchi, F., Wagner, R., 2016. The role of low-volatility organic compounds in initial particle growth in the atmosphere. Nature 533 (7604), 527.
van Pinxteren, M., Fomba, K.W., van Pinxteren, D., Triesch, N., Hoffmann, E.H., Cree, C. H., Fitzsimons, M.F., von Tümpling, W., Herrmann, H., 2019. Aliphatic amines at the Cape Verde Atmospheric Observatory: abundance, origins and sea-air fluxes. Atmos. Environ. 203, 183–195.
VanderGheynst, J.S., Cogan, D.J., DeFelice, P.J., Gossett, J.M., Walker, L.P., 1998. Effect of process management on the emission of organosulfur compounds and gaseous antecedents from composting processes. Environ. Sci. Technol. 32 (23), 3713–3718.
Vehkamäki, H., McGrath, M.J., Kurtén, T., Julin, J., Lehtinen, K.E., Kulmala, M., 2012. Rethinking the application of the first nucleation theorem to particle formation. J. Chem. Phys. 136 (9), 094107.
Wales, D.J., Doye, J.P., 1997. Global optimization by basin-hopping and the lowest energy structures of Lennard-Jones clusters containing up to 110 atoms. J. Phys. Chem. A 101 (28), 5111–5116.
Walker, M., Harvey, A.J., Sen, A., Dessent, C.E., 2013. Performance of M06, M06-2X, and M06-HF density functionals for conformationally flexible anionic clusters: M06 functionals perform better than B3LYP for a model system with dispersion and ionic hydrogen-bonding interactions. J. Phys. Chem. A 117 (47), 12590–12600.
Wang, L., Khalizov, A.F., Zheng, J., Xu, W., Ma, Y., Lal, V., Zhang, R., 2010. Atmospheric nanoparticles formed from heterogeneous reactions of organics. Nat. Geosci. 3 (4), 238.
Wang, C.-Y., Ma, Y., Chen, J., Jiang, S., Liu, Y.-R., Wen, H., Feng, Y.-J., Hong, Y., Huang, T., Huang, W., 2016. Bidirectional interaction of alanine with sulfuric acid in the presence of water and the atmospheric implication. J. Phys. Chem. A 120 (15), 2357–2371.
Wen, H., Huang, T., Wang, C.-Y., Peng, X.-Q., Jiang, S., Liu, Y.-R., Huang, W., 2018. A study on the microscopic mechanism of methanesulfonic acid-promoted binary nucleation of sulfuric acid and water. Atmos. Environ. 191, 214–226.
Xie, H.-B., Elm, J., Halonen, R., Myllys, N., Kurtén, T., Kulmala, M., Vehkamäki, H., 2017. Atmospheric fate of monoethanolamine: enhancing new particle formation of sulfuric acid as an important removal process. Environ. Sci. Technol. 51 (15), 8422–8431.
Yao, L., Garmash, O., Bianchi, F., Zheng, J., Yan, C., Kontkanen, J., Junninen, H., Mazon, S.B., Ehn, M., Paasonen, P., 2018. Atmospheric new particle formation from sulfuric acid and amines in a Chinese megacity. Science 361 (6399), 278–281.
Yoon, J.-W., Park, J.-H., Shur, C.-C., Jung, S.-B., 2007. Characteristic evaluation of electroless nickel–phosphorus deposits with different phosphorus contents. Microelectron. Eng. 84 (11), 2552–2557.
Young, L.-H., Benson, D.R., Kameel, F.R., Pierce, J.R., Junninen, H., Kulmala, M., Lee, S.-H., 2008. Laboratory studies of H 2 SO 4/H 2 O binary homogeneous nucleation from the SO 2+ OH reaction: evaluation of the experimental setup and preliminary results. Atmos. Chem. Phys. 8 (16), 4997–5016.
Yu, F., Luo, G., Liu, X., Easter, R.C., Ma, X., Ghan, S.J., 2012. Indirect radiative forcing by ion-mediated nucleation of aerosol. Atmos. Chem. Phys. 12 (23), 11451–11463.
Zhang, R., 2010. Getting to the critical nucleus of aerosol formation. Science 328 (5984), 1366–1367.
Zhang, R., Suh, I., Zhao, J., Zhang, D., Fortner, E.C., Tie, X., Molina, L.T., Molina, M.J., 2004. Atmospheric new particle formation enhanced by organic acids. Science 304 (5676), 1487–1490.
Zhang, R., Khalizov, A., Wang, L., Hu, M., Xu, W., 2011. Nucleation and growth of nanoparticles in the atmosphere. Chem. Rev. 112 (3), 1957–2011.
Zhao, Y., Truhlar, D.G., 2008. The M06 suite of density functionals for main group thermochemistry, thermochemical kinetics, noncovalent interactions, excited states, and transition elements: two new functionals and systematic testing of four M06-class functionals and 12 other functionals. Theor. Chem. Acc. 120 (1–3), 215–241.
Zheng, J., Khalizov, A., Wang, L., Zhang, R., 2010. Atmospheric pressure-ion drift chemical ionization mass spectrometry for detection of trace gas species. Anal. Chem. 82 (17), 7302–7308.
Zorn, S., Drewnick, F., Schott, M., Hoffmann, T., Borrmann, S., 2008. Characterization of the South Atlantic marine boundary layer aerosol using an aerodyne aerosol mass spectrometer. Atmos. Chem. Phys. 8 (16), 4711–4728.